Research Square

Preprints are preliminary reports that have not undergone peer review.
They should not be considered conclusive, used to inform clinical practice,
or referenced by the media as validated information.

Flexible Carbon Nanotube-based Terahertz Devices for Next-generation Wireless Communications

Li Ding

lding@pku.edu.cn

Peking University https://orcid.org/0000-0003-4310-9957

Yan Li

Peking University

Mingyue Fu

Peking University

Weifeng Wu

Peking University

Xiaowei He

Peking University

Rui Chen

National Space Science Center, Chinese Academy of Sciences

Jiawei Han

Sheng Wang

Peking University https://orcid.org/0000-0003-2605-2768

Article

Keywords: aligned carbon nanotube arrays, Schottky diode, flexible electronics, polyimide substrate, cutoff frequency, radiation hardened, rectifier, next generation (6G) wireless communication

Posted Date: April 27th, 2026

DOI: https://doi.org/10.21203/rs.3.rs-9323717/v1

License: This work is licensed under a Creative Commons Attribution 4.0 International License.
Read Full License

Additional Declarations: There is **NO** Competing Interest.

Flexible Carbon Nanotube-based Terahertz Devices for Next-generation Wireless Communications

Yan Li[1], Mingyue Fu[1], Weifeng Wu[1], Xiaowei He[1], Rui Chen[3,*], Jianwei Han[3], Li Ding[1,4,*], Sheng Wang[1,2,*]

[1] Key Laboratory for the Physics and Chemistry of Nanodevices and Center for Carbon-Based Electronics, School of Electronics, Peking University, Beijing, China

[2] State Key Laboratory of Photonics and Communications

[3] National Space Science Center Chinese Academy of Sciences Beijing 100190, P. R. China

[4] Chongqing Institute of Carbon-based Integrated Circuits, Peking University, Chongqing, China

[*] **Corresponding author. Email:** shengwang@pku.edu.cn (S.W.); lding@pku.edu.cn (L.D.); chenrui2010@nssc.ac.cn (R.C.)

Abstract

Next-generation wireless communication (6G), which is expected to enable far richer and unprecedented application scenarios, poses diverse challenges to conventional semiconductor technologies. These include the simultaneous requirements for high operating speed, mechanical flexibility, and radiation hardness. Fortunately, carbon nanotubes (CNTs) represent a promising emerging semiconductor that fulfills all three key attributes, owing to their intrinsic merits of high carrier mobility, exceptional mechanical flexibility, and strong covalent C-C bonding. Nevertheless, there remains a lack of experimental verification and demonstration for CNT-based flexible electronics that achieve high-speed operation and radiation hardness simultaneously. In this work, we present the first proof-of-concept demonstration of aligned carbon nanotube (ACNT)-based electronics developed for next-generation wireless communications. As a representative device architecture, we investigate ACNT-based flexible diodes exhibiting a current density exceeding 30 μA/μm, a high responsivity of 10.83 A/W, and strong nonlinearity (above 3) at near-zero bias voltage, corresponding to an intrinsic cutoff frequency of approximately 300 GHz within the terahertz regime. We further implement flexible rectifier circuits based on these

ACNT diodes, which operate at frequencies approaching 30 GHz within the millimeter-wave spectrum representing the first demonstration of such performance to date. These rectifiers cover an input power dynamic range of nearly three orders of magnitude, with a minimum detectable input power as low as −30 dBm. Furthermore, our developed flexible devices can withstand a total ionizing dose (TID) of up to 3 Mrad(Si) under ambient air conditions. Collectively, the results of this work validate that high-speed ACNT-based flexible electronics serve as a highly promising candidate platform supporting multiple critical functionalities simultaneously for future wireless communication applications.

Keywords: aligned carbon nanotube arrays, Schottky diode, flexible electronics, polyimide substrate, cutoff frequency, radiation hardened, rectifier, next generation (6G) wireless communication

With the rapid evolution of wireless communication systems, higher operating frequency stands as a key prerequisite, paired with escalating demands for substantial improvements in data transmission rates and network capacity[1] . This trend spans from the sub-GHz bands of first-generation (1G) communication, to the millimeter-wave (mmWave) spectrum employed in current 5G networks, and further toward the terahertz (THz) regime targeted for upcoming 6G systems in the near future. Beyond transmission speed, the architecture of wireless communication has gradually evolved[1] from an object-centric to a human-centric network paradigm, especially in the 6G era. This shift aligns with the transition from the Internet of Things (IoT) to the Internet of Everything (IoE), which requires extending conventional technologies toward large-area and flexible electronics[2] — such as large-scale infrastructure monitoring and truly ubiquitous sensing. Furthermore, a host of novel application scenarios proposed for 6G, including three-dimensional integrated communications and unconventional data communications[1] , necessitate an upgrade from two-dimensional (near-Earth) to three-dimensional (high-altitude or even deep-space) communication systems (e.g., satellites and spacecraft), which demand radiation-resistant technologies and devices. The three aforementioned key features required for next-generation wireless communications, alongside their defined application scenarios, are illustrated in Fig. 1a.

Conventional semiconductor technologies with decades of development, such as silicon CMOS and III-V compound semiconductors, are highly mature for a wide range of electronic applications. Silicon remains the most fundamental and dominant material for integrated circuits and systems, with excellent radiation resistance, whereas III-V compound semiconductors enable the fastest solid-state devices[3], whose operating frequencies extend well into the terahertz (THz) regime. However, none of these established conventional semiconductor technologies can simultaneously satisfy all three aforementioned key performance requirements on their own. In particular, both relatively slow silicon CMOS[4] and III-V compound semiconductors face substantial challenges[5] when being adapted for large-area and flexible electronic platforms. Furthermore, from the perspective of mechanical flexibility, alternative semiconductors including IGZO, ZnO, and organic semiconductors still suffer from insufficient operating speed and often exhibit poor radiation stability, as supported by the summarized data in Tables S1 and S2 and the references cited therein. Consequently, there exists an urgent need to explore emerging semiconductor technologies, particularly low-dimensional semiconductors[5-7] such as transition metal dichalcogenides (TMDs) and carbon-based materials, as illustrated in Fig. 1b.

Among the widely investigated low-dimensional semiconductors, transition metal dichalcogenides (TMDs) have emerged[8] as a revolutionary class of two-dimensional materials. They exhibit exceptional mechanical flexibility, atomic-scale thickness, and high surface-to-volume ratio, making them attractive for numerous applications including post-silicon electronics[9], flexible sensors[10], and valleytronics[11]. In addition

to flexible device demonstrations, radiation effects up to approximately 1 Mrad have recently been characterized in TMD-based systems. Nevertheless, despite decades of research, TMD-based devices have not demonstrated superior high-frequency performance among low-dimensional semiconductors; for instance, a cutoff frequency of only 42 GHz has been reported in prior work[12]. Carbon nanotubes (CNTs) represent another leading candidate among low-dimensional semiconductors, owing to their extraordinary physical and electronic properties[13-14], and hold great promise for next-generation electronic devices. After decades of development, remarkable milestone advances have been achieved in CNT technology, spanning materials synthesis[15], transistor fabrication processes[16-18], and device structural engineering[19-20], all aimed at unlocking their full potential for future wireless communication applications. First, benefiting from ultrahigh carrier mobility, high saturation velocity, and ultra-small intrinsic capacitance, CNTs are inherently advantageous for high-speed devices[21-23]. Recent progress in fabrication optimization and device architecture innovation has even enabled power-gain cutoff frequencies (f_{max}) exceeding 1 THz[24]. Second, their robust mechanical flexibility and scalable manufacturability have been widely validated in the development of flexible systems and large-area electronics[25-28]. Third, thanks[29] to strong covalent C-C bonds, small atomic cross-section, and low atomic number, CNTs possess inherent radiation tolerance and enhanced survivability under space radiation environments. This has attracted substantial research attention toward exploring their high radiation resistance for radiation-hardened electronic applications[30-34].

As illustrated in Fig. 1, the three intrinsic properties of CNTs appear to match precisely the three key performance requirements for future wireless communication technologies. Nevertheless, nearly all reported studies have only demonstrated these three capabilities separately or in isolation. For instance, high-speed CNT-based devices with an f_{max} above 1 THz have been realized only on rigid substrates, while flexible devices lag[2] far behind with cutoff frequencies below 100 GHz. Although recent advances have reported flexible CNT devices with cutoff frequencies exceeding 100 GHz[28,35], operation within the millimeter-wave (mmWave) spectrum has still not been achieved, let alone corresponding radiation characterization. Meanwhile, radiation-hardened CNT-based devices with outstanding total ionizing dose tolerance[33,36] have been widely demonstrated, yet without any consideration or demonstration of high-speed performance. According to previous work[37], the most radiation-sensitive components are the substrate and its interface with CNTs, which undergo more severe radiation damage than gate dielectrics or the CNT channels themselves. Therefore, the radiation performance validated on rigid substrates must be re-examined and explored on flexible platforms, together with simultaneous demonstration of high-speed operation. In summary, flexible-substrate carbon nanotube devices that integrate both high-speed operation and radiation hardness must be developed and investigated to enable their practical application in next-generation wireless communication.

In this work, targeting the simultaneous integration of three key features—high speed, mechanical flexibility, and radiation resistance—for future wireless communication systems, we developed aligned carbon nanotube (ACNT)-based flexible devices with potential applications in the millimeter-wave (mmWave) spectrum, and simultaneously characterized their radiation-hardened performance (Fig. 1). To maintain focus and avoid distraction from diverse device architectures, we selected diodes as the representative device platform due to their structural simplicity. Leveraging a high-performance flexible substrate and optimized fabrication processes (see Methods for details), we fabricated flexible ACNT-based Schottky barrier diodes (ACNT-FSBDs) exhibiting a current density exceeding 30 μA/μm, together with outstanding responsivity (10.83 A/W) and nonlinearity (>3) at very low bias voltages. These characteristics enable superior rectification performance and low power consumption. Using standard radio-frequency (RF) characterizations, we extracted an intrinsic cutoff frequency of nearly 300 GHz for our flexible ACNT diodes, extending into the terahertz regime. We further constructed flexible rectifier circuits based on these terahertz-capable ACNT-FSBDs and demonstrated operation at frequencies close to 30 GHz (within the mmWave spectrum). The devices enable rectification at an ultra-low RF input power of −30 dBm and cover a dynamic range of nearly three orders of magnitude, satisfying the requirements for both IoT/IoE and high-speed applications envisioned in 6G communication — even outperforming conventional semiconductor technologies. Finally, the ACNT-based flexible devices were evaluated under total ionizing dose (TID) irradiation up to 3 Mrad(Si) in ambient air. This level of radiation tolerance is comparable to that of other material systems, even those on rigid substrates, and remains highly competitive when combined with the demonstrated high-speed performance.

Results

Characterization of Flexible ACNT based Diodes

Aligned carbon nanotube (ACNT) arrays were employed as the channel material for the diodes, fabricated via the previously developed dimension-limited self-alignment (DLSA)[38] method. The resulting high-purity ACNT array films exhibit a density in excess of 100 CNTs per micrometer, as shown in the scanning electron microscopy (SEM) micrograph (Fig. S1a). However, polymeric residues on the CNT surface introduced by solution-based purification processes can severely degrade the contact and gate interface quality between ACNTs and metal electrodes/dielectric layers, leading to a significant reduction in device performance. To address this issue, a yttrium oxide coating and de-coating (YOCD) process[39] combined with vacuum annealing was employed, which effectively mitigates polymeric residues on the CNT surface prior to device fabrication (details provided in the Methods section). After this treatment, Raman spectroscopy characterization (Fig. S1b) of the CNTs yielded a G/D ratio of 33.12, indicating a substantial reduction in structural defects attributable to the YOCD and annealing process.

Polyimide (PI) film, a material renowned for its exceptional electrical insulation and mechanical robustness, was selected as the flexible substrate to fabricate devices with superior flexibility and bending fatigue resistance[40]. Prior to ACNT array transfer, the flexible substrate was surface-modified by spin-coating a thin layer of hydrophilic PI precursor solution followed by deposition of a thin HfO_2 film; this modification enhances the adhesion between ACNT films and the flexible substrate, thus improving the quality of ACNT films during the transfer process (details in the Methods section). The detailed fabrication process for the flexible ACNT diode is provided in the Methods section and Supporting Information Fig. S2; this process is adapted from the rigid-substrate fabrication protocol with tailored optimizations for flexible substrates. In the design of the flexible ACNT diode (Figs. 2a and 2b), palladium (Pd) was used as the anode material to form a p-type ohmic contact, while titanium (Ti) served as the cathode material to form a Schottky contact—consistent with our previous work[41,42]. Ground-signal-ground (GSG) pads with a Ti/Au stack were fabricated for radio-frequency (RF) characterizations. The final physical layout and SEM micrographs of the flexible ACNT-based Schottky diode are presented in Fig. S3, including a magnified view of the device channel.

Fig. 2c shows the typical direct current (DC) I – V characteristics of a flexible ACNT diode with a 200 nm channel length and a 60 μm channel width. At a forward bias of 1 V, the diode exhibited a measured current density of 30.89 $\mu A\ \mu m^{-1}$ (defined as current divided by channel width). Fig. S4 presents the statistical distribution of the current density measured at a 1 V forward bias. The band alignment of the Schottky diode is illustrated in the inset of Fig. 2c, with the observed forward current conduction and reverse current blocking behaviour consistent with the measured DC characteristics. To further characterize the diode's electrical performance, we simulated and fitted the measured data using a diode model[24]. The Shockley diode equation employed for this fitting is expressed as follows:

$$I = I_S\left[e^{\frac{q(V-IR_S)}{nkT}} - 1\right] + \frac{V-IR_S}{R_{sh}} \qquad (1)$$

where n is the ideality factor, typically between 1 and 2, k is the Boltzmann constant, T is the temperature, $I_S$is the reverse saturation current, R_S is the series resistance, and R_{sh} is the shunt resistance. Fitting the experimental data yielded an ideality factor n of 2.45, a value lower than those reported for MoS_2-based Schottky diodes[5].

We further benchmarked our ACNT-based flexible diodes against state-of-the-art devices based on diverse materials and technologies — ranging from conventional semiconductors to emerging low-dimensional materials—as shown in Fig. 2d. Our champion flexible diode, with a current density of 30.89 $\mu A\ \mu m^{-1}$, outperforms not only diodes based on emerging two-dimensional materials (graphene: $4.89 \times 10^{-2}\ \mu A\ \mu m^{-1}$; MoS_2: 3.11 $\mu A\ \mu m^{-1}$) but also oxide- and organic-semiconductor diodes (ZnO: 4.52

$\times 10^{-4}$ μA μm^{-1}; IGZO: 2.53 $\times 10^{-3}$ μA μm^{-1}), even when these reference devices are fabricated on rigid substrates. Notably, the performance of our diodes is even comparable to that of conventional GaAs-based semiconductor diodes, an enhancement attributable to the intrinsically high carrier mobility of ACNTs and our optimized fabrication processes.

Beyond the fundamental DC I – V performance, two key diode parameters—responsivity (R_i) and nonlinearity (NL)—are critical for the rectification performance of rectifier circuits. Current responsivity quantifies a diode's ability to generate a DC output current from a given RF input power in rectifier circuits, while nonlinearity (a metric describing deviation from ohmic linear conduction) is defined as the ratio of differential conductance to static conductance. Both parameters can be calculated using the following equations[43,44]:

$$R_i = \frac{I_{d.c.}}{P_{in}} = \frac{\left.\frac{d^2I}{dV^2}\right|_{V=V_0}}{2\left.\frac{dI}{dV}\right|_{V=V_0}} \quad (2)$$

$$NL(V) = \frac{\frac{dI}{dV}(V)}{\frac{I(V)}{V}} \quad (3)$$

where V_0 denotes the operating bias point. The calculated responsivity and nonlinearity values are both plotted in Fig. 2e. The flexible ACNT diode achieves a maximum responsivity of 10.83 A W^{-1}, which exceeds that of random-network CNT-based Schottky diodes fabricated on silicon substrates[42]. The nonlinearity of our device exceeds 3, a threshold value required for high-performance rectification[44]. Notably, the diode exhibits excellent rectification performance (derived from its DC characteristics) at a bias voltage of approximately 0.1 V—near zero bias—affording a significant low-power consumption advantage (Fig. 2e).

To systematically characterize the high-frequency performance of the flexible ACNT diode, we performed scattering parameter (S-parameter) measurements using a vector network analyzer (VNA). Fig. 3a depicts the small-signal equivalent circuit model of the ACNT-FSBD, which was used for simulation and electrical parameter extraction. Fig. 3b presents the measured S-parameters over the frequency range of 100 MHz to 40 GHz, alongside the simulated S-parameter results; the fitted results based on the fequivalent circuit model in Fig. 3a show excellent agreement with the experimental S-parameter data. Fig. S5 provides further insights into the impedance characteristics governing the high-frequency behaviour of the flexible ACNT diode. The Smith chart measured at 0 V bias for a diode with a 20 μm channel width and 200 nm channel length exhibits good agreement with the Advanced Design System (ADS) simulation results, validating the extracted equivalent circuit model. Additionally, the frequency-dependent resistance and capacitance extracted over 100 MHz to 40 GHz elucidate the evolution of parasitic components in the diode at high frequencies. From the S-parameter measurements, we extracted the device's intrinsic cutoff

frequency (a metric of ultimate speed, without de-embedding) using two independent methods: simulation[41] and impedance intersection[45]. The intrinsic cutoff frequency (f_C) is defined[5] as the maximum frequency at which the diode can effectively propagate electrical signals. This metric reflects the intrinsic speed of the diode, determined by the junction resistance (R_j), junction capacitance (C_j), and series resistance (R_s); it neglects parasitic transmission losses, load resistance, and impedance-matching losses that are inherent to practical rectifier circuits. For the first method, we performed ADS electromagnetic simulations using the equivalent circuit model illustrated in Fig. 3a, which rigorously accounts for Schottky junction capacitance and the impact of parasitic elements on the device's dynamic electrical behaviour. The intrinsic cutoff frequency is defined by Equation[5] as:

$$f_c = \frac{\sqrt{1+\frac{R_j}{R_s}}}{2\pi R_j C_j} \qquad (4)$$

The key electrical parameters extracted via experimental fitting are: series resistance R_s = 10 Ω, junction resistance R_j = 10 kΩ, and junction capacitance C_j = 1.5 fF. From these values, the intrinsic cutoff frequency of the ACNT-based flexible diode is calculated to be 335.7 GHz, extending into the terahertz (THz) regime. To validate this fC result, we also extracted the intrinsic cutoff frequency using the second method, where fC is defined[5,42,45,46] as the frequency at which the real (resistive) and imaginary (reactive) components of the device impedance intersect. Using this method, we extracted an intrinsic cutoff frequency of approximately 295 GHz (Fig. 3c), which falls within the THz regime and is consistent with the simulation-derived value.

A benchmark comparison of intrinsic cutoff frequencies is presented in Fig. 3d, where we compare our device against state-of-the-art diodes fabricated on both rigid and flexible substrates across a broad range of materials and technologies. Our device's intrinsic cutoff frequency of ~300 GHz is clearly superior to that of diodes based on other materials, and even outperforms diodes fabricated using conventional III-V compound semiconductor technology. This exceptional high-speed performance highlights the great potential of ACNT-based flexible electronics for wearable devices and terahertz communication systems. Notably, the diode's channel width was designed to be ~60 μm in this work to optimize rectifier circuit performance; this cutoff frequency can be further enhanced by scaling down the channel width.

Flexible ACNT based Rectifier Circuits

Building on the developed terahertz flexible ACNT diode, we have further fabricated flexible rectifier circuits to evaluate their rectification performance for the demonstration of high-speed flexible circuits. The detailed measurement setup is depicted in Fig. 4a, which monitors the rectified current response by detecting the output voltage across the load while varying the input signal frequency and power level.

Leveraging these terahertz diodes, we first characterized the maximum operating frequency of our flexible rectifier circuits to derive their bandwidth for high-speed applications. By definition[6,42], the maximum operating frequency of a rectifier is the frequency at which the DC output voltage drops to $1/\sqrt{2}$ of its low-frequency peak value. In contrast to the intrinsic cutoff frequency of diodes, the operating frequency and bandwidth of the rectifier account for impedance-matching losses in the circuit, thus reflecting the practical attainable operating frequency under actual working conditions. As illustrated in Fig. 4b, we measured the output voltage of our flexible rectifier by sweeping the frequency from 10 to 40 GHz at RF input powers of -10, -2, 0, and 3 dBm under zero DC bias—a condition tailored for low-power IoT and sensor applications. We clearly demonstrate that, for the first time, the flexible rectifier achieves a maximum operating frequency of 28.6 GHz at an input power of 0 dBm, extending into the millimeter-wave (mmWave) spectrum on a flexible substrate. Fig. S6 presents a statistical analysis of the extrinsic cutoff frequency ($f_{c,ext}$) of the CNT-FSBDs. The corresponding histogram quantifies the distribution of $f_{c,ext}$ extracted under zero bias, with the minimum $f_{c,ext}$ at approximately 20 GHz. Notably, the rectifier achieves not only an ultrahigh mmWave operating frequency but also a relatively large DC output amplitude exceeding 250 mV even at 30 GHz, outperforming all reported[45] ZnO-based rectifiers to date. Additional characterizations, including the DC output voltage as a function of DC bias and RF input power, are presented in Fig. S7 of the Supporting Information.

Second, for ubiquitous sensing in the Internet of Everything (IoE) architecture—particularly for flexible electronics—low-power operation is a critical design criterion for both devices and circuits. Demonstrating rectifier performance solely under zero DC bias is insufficient; thus, we further characterized its operation under ultra-low RF input powers. As shown in Fig. 4c, we measured the output voltage of the flexible rectifier at RF input powers scaled down to as low as -30 dBm, with a vector network analyzer applying operating frequencies ranging from 0.8 GHz to 20 GHz. It is evident that a minimum DC output voltage of 12 mV is achievable at the highest operating frequency with an input RF power as low as -30 dBm, and the DC output voltage rises rapidly with increasing RF input power. Notably, the -30 dBm input RF power demonstrated here is at least one order of magnitude lower than that reported[5] in previous WiFi signal energy harvesting studies—even integrating antenna structures—and is very close to the power levels of cellular and WiFi signal propagation in ambient air for daily wireless communication scenarios (typically below -40 dBm). Fig. S7b further illustrates the DC output voltage of the flexible rectifier across a broad RF input power range. The DC output voltage was measured as a function of RF input power from −30 to 3 dBm at multiple operating frequencies spanning 800 MHz to 20 GHz under zero-bias conditions, which highlights the frequency-dependent rectification behavior and the rapid voltage increase with rising RF input power.

In addition to characterizing speed (mmWave operating frequency) and low-power operation (battery-free power harvesting at RF inputs as low as -30 dBm under zero DC bias), we further characterized the dynamic range of the flexible rectifier—defined as the RF input power range over which the output voltage maintains a linear relationship with the input power. To this end, we measured the DC output voltage of the flexible rectifier over the widest possible RF input power range at a representative operating frequency of 10 GHz, as shown in Fig. 4d. The flexible rectifier achieves a dynamic range of RF input power from -24 dBm to 4 dBm, spanning nearly three orders of magnitude (28 dB) and thus bridging the power regimes explored in the high-frequency demonstration (Fig. 4b) and low-power characterization (Fig. 4c). For comparison, the performance of rectifiers based on alternative technologies or fabricated on rigid substrates is also plotted in Fig. 4d. We clearly show that, in comparison with these state-of-the-art rectifiers[5,42,45], our flexible rectifier exhibits both the largest dynamic range and the highest output voltage—a testament to its exceptional rectification efficiency stemming from the superior responsivity and nonlinearity of the flexible ACNT diode under zero bias.

Furthermore, to emphasize the groundbreaking speed advancement of our flexible rectifier for high-frequency flexible circuit applications, we benchmarked its operating frequency (Fig. 4e) against other reported rectifiers based on alternative materials and technologies—including metal oxides (e.g., ZnO, IGZO), 2D materials (e.g., tungsten diselenide (WSe_2), transition metal dichalcogenides (TMDs)), silicon-based materials, and organic semiconductors—with relevant data summarized in Table S1 and the associated references. Leveraging the terahertz flexible ACNT diode, our flexible rectifier achieves a maximum operating frequency in the mmWave spectrum—the highest value reported to date—outperforming all previously reported rectifiers, even those fabricated on rigid substrates (hollow symbols in Fig. 4e) or based on conventional semiconductors. This unprecedented speed advancement lays a cutting-edge foundation for the development of next-generation high-frequency flexible electronics.

Total Ionizing Dose Characterization

Finally, to validate the radiation tolerance of the terahertz flexible devices developed in this work (fabricated via the same process and device architecture), we conducted characterization for flexible radiation-hardened applications in the 6G era. Prior studies[33] have demonstrated that ACNT-based devices possess inherent radiation-hardened properties due to their exceptional physical characteristics, and the substrate is typically the most radiation-susceptible component in such devices. However, the polyimide (PI) substrate selected in this work—among a range of flexible substrates—exhibits structural advantages for radiation-hardened applications[47,48], including charge recombination and self-healing capabilities. By combining the inherent advantages of carbon nanotubes and the PI substrate, we performed total ionizing dose (TID) irradiation tests on the flexible ACNT diodes, which were exposed to cumulative doses of up

to 3 Mrad (Si) at a dose rate of 330 rad (Si)/s via Co-60 γ-rays in ambient air (Fig. 5a). Fig. S8 schematically illustrates the experimental setup for the TID radiation-hardness tests. The multi-hole sample stage enables the simultaneous irradiation of distinct device regions with precisely defined cumulative doses, facilitating the controlled and reproducible assessment of radiation tolerance in the flexible ACNT diodes. A comparison of device performance before and after irradiation (Fig. 5b) reveals that only a slight statistical variation in current is observed, with the device retaining its pre-irradiation performance without significant degradation.

Benchmarking results are also presented in Fig. 5c, where we compare the maximum TID tolerance of devices fabricated from various semiconductor materials—including GaAs-Si, Si, IGZO, GaAs, and carbon nanotubes—under total-dose irradiation, with relevant data compiled in Table S1 and the associated references. The results demonstrate that flexible CNT-based devices exhibit radiation tolerance comparable to that of silicon (Si) and superior to that of other conventional semiconductors—even those fabricated on rigid substrates. Notably, the TID tolerance reported previously for carbon nanotube-based devices on rigid substrates is higher than that demonstrated here; however, the synergistic combination of high operating speed and radiation tolerance in a flexible platform renders our flexible ACNT diode superior overall. Collectively, the results in Fig. 5 demonstrate that the devices developed in this work hold great potential for radiation-exposed environments such as space missions, as well as nuclear and aerospace applications[49].

Conclusion

We report ACNT-based flexible devices and circuits that simultaneously exhibit high-speed and radiation-tolerant performance, meeting the core requirements of next-generation wireless communication. Thanks to the tailored treatment process for PI substrates and the optimized, scalable fabrication procedure for CNT devices, we have successfully fabricated flexible ACNT diodes with a high current density of 30.89 μA/μm, an excellent responsivity of 10.83 A/W, and a strong nonlinearity (in excess of 3). RF characterization results confirm an intrinsic cutoff frequency (f_c) of approximately 300 GHz extending into the terahertz regime, a value validated by two independent extraction methods: simulation (335.7 GHz) and the intersection method (295 GHz). Furthermore, we constructed flexible rectifier circuits using our developed flexible ACNT diodes. For the first time, these flexible circuits achieve an operating frequency of nearly 30 GHz in the millimeter-wave (mmWave) spectrum, outperforming circuits based on alternative technologies—including those fabricated from conventional semiconductors or on rigid substrates. Leveraging the superior DC performance at near-zero bias voltage, ACNT-based flexible rectifiers also enable ultra-low-power signal rectification and energy harvesting, with a minimum input power of -30 dBm that matches the power levels of ambient wireless signals. Additionally, they exhibit an ultra-broad dynamic range of -24 dBm to 4 dBm, corresponding to nearly three orders of magnitude variation in input power.

Moreover, these terahertz-capable ACNT-based flexible devices were subjected to total ionizing dose (TID) irradiation tests with a cumulative dose of up to 3 Mrad (Si) to verify their radiation-hardened performance. Collectively, the findings of this work demonstrate that ACNT-based electronics realize a terahertz-scale f_c for high-speed wireless communication, a flexible form factor for seamless integration into the Internet of Everything (IoE), and radiation tolerance for 3D integrated communication systems—all critical requirements for next-generation wireless communication.

This work underscores the tremendous potential of ACNT-based electronics for future wireless communication applications and lays a solid foundation for a versatile semiconductor technology that delivers a viable solution for a diverse range of electronic applications. This single technology enables easier integration of multifunctional capabilities and optimized form factors for various devices and circuits. However, future research efforts should focus on advancing ACNT material synthesis and process optimization on flexible substrates to further boost device performance. Most importantly, universal electronic devices such as transistors need to be developed and characterized to enrich the portfolio of ACNT-based devices, expand circuit functionality, and ultimately pave the way for more comprehensive and practical ACNT-based electronic systems tailored for next-generation wireless communication.

Methods

Preparation of CNT Films

In this work, high-purity semiconducting ACNT arrays were successfully fabricated using multiple dispersion and DLSA techniques[38]. During the subsequent fabrication of flexible CNT-based RF diodes, the presence of PCz organic molecules introduced significant barriers between the CNTs and the electrodes, leading to a noticeable increase in contact resistance. To address this issue, an yttrium oxide (Y_2O_3) coating was applied to the device prior to fabrication, followed by a YOCD process to remove PC_z molecules and other organic/inorganic contaminants from both the surface of the CNT films and the surrounding substrate. Additionally, a vacuum annealing treatment at 500°C for 10 minutes was performed to further decompose any remaining PCz molecules on the CNT surface, significantly improving the contact quality and reducing contact resistance.

Fabrication of the CNT RF Diodes

The fabrication process of the diodes is schematically illustrated in Fig. S2, and is described as follows:1) A 125 μm thick PI films were prepared by spin-coating liquid PI precursor (ZKPI-3022S) onto the PI substrate at 4500 rpm. The coated films were subsequently subjected to a multi-step curing process: 140 °C for 20 min, 200 °C for 30 min, and 300 °C for 4 h, to ensure full imidization and mechanical stability. After curing, a 7 nm HfO_2 dielectric layer was deposited on the PI surface using atomic layer deposition (ALD). The processed PI film was adhered to a silicon (Si) substrate using double-sided PI tape to serve as the

support layer for the device. 2)The CNT film was transferred onto the treated PI substrate. During the transfer, a 1:6 volume ratio of hydrofluoric acid (HF) solution was used, and a 500 nm thick polymethyl methacrylate (PMMA) protection layer was spin-coated at 2000 rpm on the CNT film surface. After the transfer was completed, the PMMA layer was removed by soaking in acetone, successfully stripping the protective layer and completing the CNT film transfer. 3)The device pattern was defined on the CNT film on the PI substrate using electron-beam lithography (e-beam lithography, EBL). Then, a 5 nm Ti layer and a 90 nm Au layer were sequentially deposited using e-beam evaporation to form the DC test contact pads. After metal deposition, a standard lift-off process was applied to remove the unexposed metal, completing the transfer of the electrode pattern. 4)Excess CNTs outside the device channel were removed using oxygen plasma etching for 35 seconds. This step effectively eliminates the unwanted CNTs in the non-channel regions, ensuring the precision of the device structure. 5)To form the ohmic contact on the CNTs, a 30 nm Pd layer and a 60 nm Au layer were deposited sequentially via e-beam evaporation. For the Schottky contact, a 30 nm Ti layer and a 60 nm Au layer were deposited. All metal layers were deposited using the lift-off process to remove the excess metal, ensuring the precise transfer of the electrode structures. 6)A 500 nm thick PMMA was used as the e-beam positive resist for defining the source-drain (S-D) electrode structure. Using e-beam evaporation, a 200 nm thick Ti/Au bilayer metal was deposited. After the metal deposition, the lift-off process was applied to remove the excess metal, resulting in the formation of the complete source-drain electrode structure.

Measurement of the CNT RF Diodes—D.C. Measurements

The current-voltage (I-V) characteristics of the flexible CNT radio-frequency diodes were measured using a Keithley 4200 Semiconductor Characterization System. This instrument provides high-precision current and voltage measurements, ensuring accurate evaluation of the diode performance.

Measurement of the CNT RF Diodes—S-parameter Measurements

S-parameter measurements were performed using a probe station (SUSS PA200), GSG probes, coaxial cables, a vector network analyzer (HP 8510C) with a frequency range of 100 MHz to 50 GHz, and a signal generator (Agilent N5183A) to measure the single-port scattering parameter (S_{11}). To ensure accurate measurements, a short-open-load-through (SOLT) calibration procedure was used to calibrate the GSG probes and coaxial RF cables. The bias for the flexible CNT radio-frequency diode was provided by a tunable source (HP 4142B) with a voltage range of 0 to ±0.6 V, enabling bias sweep. The real and imaginary parts of the S_{11} parameter were measured and recorded using an S-parameter test module (AV3645).

Measurement of the CNT RF Diodes—Rectifier Circuit Measurements

For the measurement of the rectifier output voltage (Vout) shown in Fig. 4, the signal generator (Agilent N5183A, frequency range: 100 MHz to 50 GHz) was connected to a bias tee. The output voltage of the

rectifier was measured across a 10 MΩ load resistor to simulate real-world loading conditions. This setup allowed for the recording of the rectifier's output characteristics at various frequencies.

Measurement of the Total Ionizing Dose

Prior to irradiation, the flexible Schottky diodes were stored in a vacuum environment to minimize the effects of moisture and oxygen from the ambient air on the diode performance. The equipment schematic diagram is shown in Figure S6a. The irradiation experiment was conducted using a Co-60 γ-ray source. The irradiation dose rate was controlled to 333.33 rad (Si) s^{-1} by adjusting the distance between the sample and the Co-60 γ-ray source. After 150 minutes of irradiation, the total dose accumulated by the sample reached 3 Mrad (Si). Following irradiation, the device was allowed to stabilize for a period of time, after which the current-voltage (I-V) characteristics of the diode were measured using a Keithley 4200 Semiconductor Characterization System.

References

1. Dang S., Amin O., Shihada B., Alouini M. S. What should 6G be? *Nat. Electron.* **3**, 20-29 (2020).
2. Zhang H.*, et al.* Flexible and Stretchable Microwave Electronics: Past, Present, and Future Perspective. *Adv. Mater. Technol.* **6**, 2000759 (2021).
3. Mei X.*, et al.* First demonstration of amplification at 1 THz using 25-nm InP high electron mobility transistor process. *IEEE Electron Device Lett.* **36**, 327-329 (2015).
4. Passi V., Raskin J.-P. Review on analog/radio frequency performance of advanced silicon MOSFETs. *Semicond. Sci. Technol.* **32**, 123004 (2017).
5. Zhang X.*, et al.* Two-dimensional MoS2-enabled flexible rectenna for Wi-Fi-band wireless energy harvesting. *Nature.* **566**, 368-372 (2019).
6. Zhang J., Li Y., Zhang B., Wang H., Xin Q., Song A. Flexible indium–gallium–zinc–oxide Schottky diode operating beyond 2.45 GHz. *Nat. Commun.* **6**, 7561 (2015).
7. Novoselov K. S.*, et al.* Electric field effect in atomically thin carbon films. *Science.* **306**, 666-669 (2004).
8. Zheng F. Y., Meng W. Q., Li L. J. Continue the Scaling of Electronic Devices with Transition Metal Dichalcogenide Semiconductors. *Nano Letters.* **25**, 3683-3691 (2025).
9. Zhang X., Zhao H., Wei X., Zhang Y., Zhang Z., Zhang Y. Two-dimensional transition metal dichalcogenides for post-silicon electronics. *National Science Open.* **2**, 20230015 (2023).
10. Aftab S., Al-Kahtani A. A., Iqbal M. Z., Hussain S., Koyyada G. Recent Advances in 2D Wearable Flexible Sensors. *Adv. Mater. Technol.* **8**, 2202168 (2023).
11. Liu Y., Gao Y., Zhang S., He J., Yu J., Liu Z. Valleytronics in transition metal dichalcogenides materials. *Nano Research.* **12**, 2695-2711 (2019).
12. Cheng R.*, et al.* Few-layer molybdenum disulfide transistors and circuits for high-speed flexible electronics. *Nat. Commun.* **5**, 5143 (2014).
13. De Volder M. F., Tawfick S. H., Baughman R. H., Hart A. J. Carbon nanotubes: present and future commercial applications. *Science.* **339**, 535-539 (2013).
14. Rutherglen C., Jain D., Burke P. Nanotube electronics for radiofrequency applications. *Nature nanotechnology.* **4**, 811-819 (2009).
15. Ze Y., Liu Y., Wang B., Yin H., Jin C., Zhang Z. Carbon nanotube materials for future integrated circuit applications. *Materials Today.* **79**, 97-111 (2024).
16. Martel R., Schmidt T., Shea H., Hertel T., Avouris P. Single-and multi-wall carbon nanotube field-effect transistors. *Appl. Phys. Lett.* **73**, 2447-2449 (1998).
17. Che Y.*, et al.* Self-aligned T-gate high-purity semiconducting carbon nanotube RF transistors operated in quasi-ballistic transport and quantum capacitance regime. *ACS nano.* **6**, 6936-6943 (2012).
18. Javey A., Tu R., Farmer D. B., Guo J., Gordon R. G., Dai H. High performance n-type carbon nanotube field-effect transistors with chemically doped contacts. *Nano letters.* **5**, 345-348 (2005).
19. Allen B. L., Kichambare P. D., Star A. Carbon nanotube field‐effect‐transistor‐based biosensors. *Adv. Mater.* **19**, 1439-1451 (2007).
20. Li H., Liao Y., Zhang F., Sun T., Liu X., Chen S. A Carbon Nanotube Transistor Based on Buried-Gate Structure. *Materials.* **18**, 218 (2025).
21. Si J., Zhang P., Zhang Z. Road map for, and technical challenges of, carbon-nanotube integrated circuit technology. *National Science Review.* **11**, nwad261 (2024).
22. Zhang Z., Zhang N., Zhang Z. High-Performance Carbon Nanotube Electronic Devices: Progress and Challenges. *Micromachines.* **16**, 554 (2025).
23. Kreupl F.*, et al.* Carbon nanotubes in microelectronic applications. In: *Physics, Chemistry And Application Of Nanostructures: Reviews and Short Notes to Nanomeeting 2003*). World Scientific (2003).

24. Manohara H. M., Wong E. W., Schlecht E., Hunt B. D., Siegel P. H. Carbon nanotube Schottky diodes using Ti− Schottky and Pt− Ohmic contacts for high frequency applications. *Nano letters.* **5**, 1469-1474 (2005).
25. Cao Q.*, et al.* Medium-scale carbon nanotube thin-film integrated circuits on flexible plastic substrates. *Nature.* **454**, 495-500 (2008).
26. Sun D.-M.*, et al.* Mouldable all-carbon integrated circuits. *Nat. Commun.* **4**, 2302 (2013).
27. Tang J.*, et al.* Flexible CMOS integrated circuits based on carbon nanotubes with sub-10 ns stage delays. *Nat. Electron.* **1**, 191-196 (2018).
28. Long G.*, et al.* Carbon nanotube-based flexible high-speed circuits with sub-nanosecond stage delays. *Nat. Commun.* **13**, 6734 (2022).
29. Krasheninnikov A., Nordlund K. Ion and electron irradiation-induced effects in nanostructured materials. *Journal of applied physics.* **107**, 071301 (2010).
30. McMorrow J. J., Cress C. D., Gaviria Rojas W. A., Geier M. L., Marks T. J., Hersam M. C. Radiation-hard complementary integrated circuits based on semiconducting single-walled carbon nanotubes. *ACS nano.* **11**, 2992-3000 (2017).
31. Wang Y., Xiao L. Repairable integrated circuits for space. *Nat. Electron.* **3**, 586-587 (2020).
32. Zhao Y.*, et al.* Radiation effects and radiation hardness solutions for single-walled carbon nanotube-based thin film transistors and logic devices. *Carbon.* **108**, 363-371 (2016).
33. Zhu M. G.*, et al.* Radiation-hardened and repairable integrated circuits based on carbon nanotube transistors with ion gel gates. *Nat. Electron.* **3**, 622-629 (2020).
34. Zhu M. G., Zhang Z., Peng L. M. High‐performance and radiation‐hard carbon nanotube complementary static random‐access memory. *Adv. Electron. Mater.* **5**, 1900313 (2019).
35. Wang Y. R.*, et al.* Sub-180-nanometer-thick ultraconformable high-performance carbon nanotube-based dual-gate transistors and differential amplifiers. *Science Advances.* **10**, eadq6022 (2024).
36. Wang X.*, et al.* Ultralow-Power and Radiation-Tolerant Complementary Metal-Oxide-Semiconductor Electronics Utilizing Enhancement-Mode Carbon Nanotube Transistors on Paper Substrates. *Adv. Mater.* **34**, 2204066 (2022).
37. Zhu M., Zhou J., Sun P., Peng L.-M., Zhang Z. Analyzing Gamma-Ray Irradiation Effects on Carbon Nanotube Top-Gated Field-Effect Transistors. *ACS Appl. Mater. Interfaces.* **13**, 47756-47763 (2021).
38. Liu L. J.*, et al.* Aligned, high-density semiconducting carbon nanotube arrays for high-performance electronics. *Science.* **368**, 850-856 (2020).
39. Ma Z., Han J., Yao S., Wang S., Peng L.-M. Improving the performance and uniformity of carbon-nanotube-network-based photodiodes via yttrium oxide coating and decoating. *ACS Appl. Mater. Interfaces.* **11**, 11736-11742 (2019).
40. Chisca S., Sava I., Musteata V.-E., Bruma M. Dielectric and conduction properties of polyimide films. In: *CAS 2011 Proceedings (2011 International Semiconductor Conference)*). IEEE (2011).
41. Zhang Z.*, et al.* Terahertz Schottky Barrier Diodes Based on Aligned Carbon Nanotube Arrays. *IEEE Electron Device Lett.* **44**, 845-848 (2023).
42. Xue C. Q., Wu W. F., Yang Y. J., Zhou J. S., Ding L., Wang S. Carbon Nanotube Diodes Operating at Frequencies of Over 50 GHz. *Small.* 2207628 (2023).
43. Pozar D. *Microwave Engineering [Edn 4th]* (2012).
44. Citroni R., Di Paolo F., Livreri P. Progress in THz rectifier technology: Research and perspectives. *Nanomaterials.* **12**, 2479 (2022).
45. Georgiadou D. G.*, et al.* 100 GHz zinc oxide Schottky diodes processed from solution on a wafer scale. *Nat. Electron.* **3**, 718-725 (2020).
46. Semple J., Georgiadou D. G., Wyatt-Moon G., Gelinck G., Anthopoulos T. D. Flexible diodes for radio frequency (RF) electronics: a materials perspective. *Semicond. Sci. Technol.* **32**, 123002 (2017).

47. Plis E. A., Engelhart D. P., Cooper R., Johnston W. R., Ferguson D., Hoffmann R. Review of radiation-induced effects in polyimide. *Appl. Sci.* **9**, 1999 (2019).
48. O'Donnell J., Whittaker A. The high resolution 13C NMR spectrum of poly (N, N′ -bis (phenoxyphenyl) pyromellitimide),(Kapton). *Polym. Bull.* **12**, 319-325 (1984).
49. Duzellier S. Radiation effects on electronic devices in spaces. *Aerosp. Sci. Technol.* **9**, 93-99 (2005).

Data availability

The data that support the plots within this paper and other findings of this study are available from the corresponding authors upon reasonable request.

Acknowledgements

This work was supported by the National Science Foundation of China (Grant No. 62571005, 62275003, U21A6004) and Peking Nanofab.

Author contributions

S.W. and L.D. proposed and supervised the project. S.W. designed the experiment. Y.L. performed the fabrication of the CNT diodes and the performance measurement. M.F. and W.W. are helpful for the fabrication of the CNT diodes and the performance measurement. Y.L., R.C., L.D. and S.W. analyzed the data and co-wrote the manuscript. All authors discussed the results and contributed to manuscript preparation.

Competing interests

The authors declare no competing interests.

Additional Information

Supporting Information, **Figure S1** to **S8, Table S1** to **S2**.

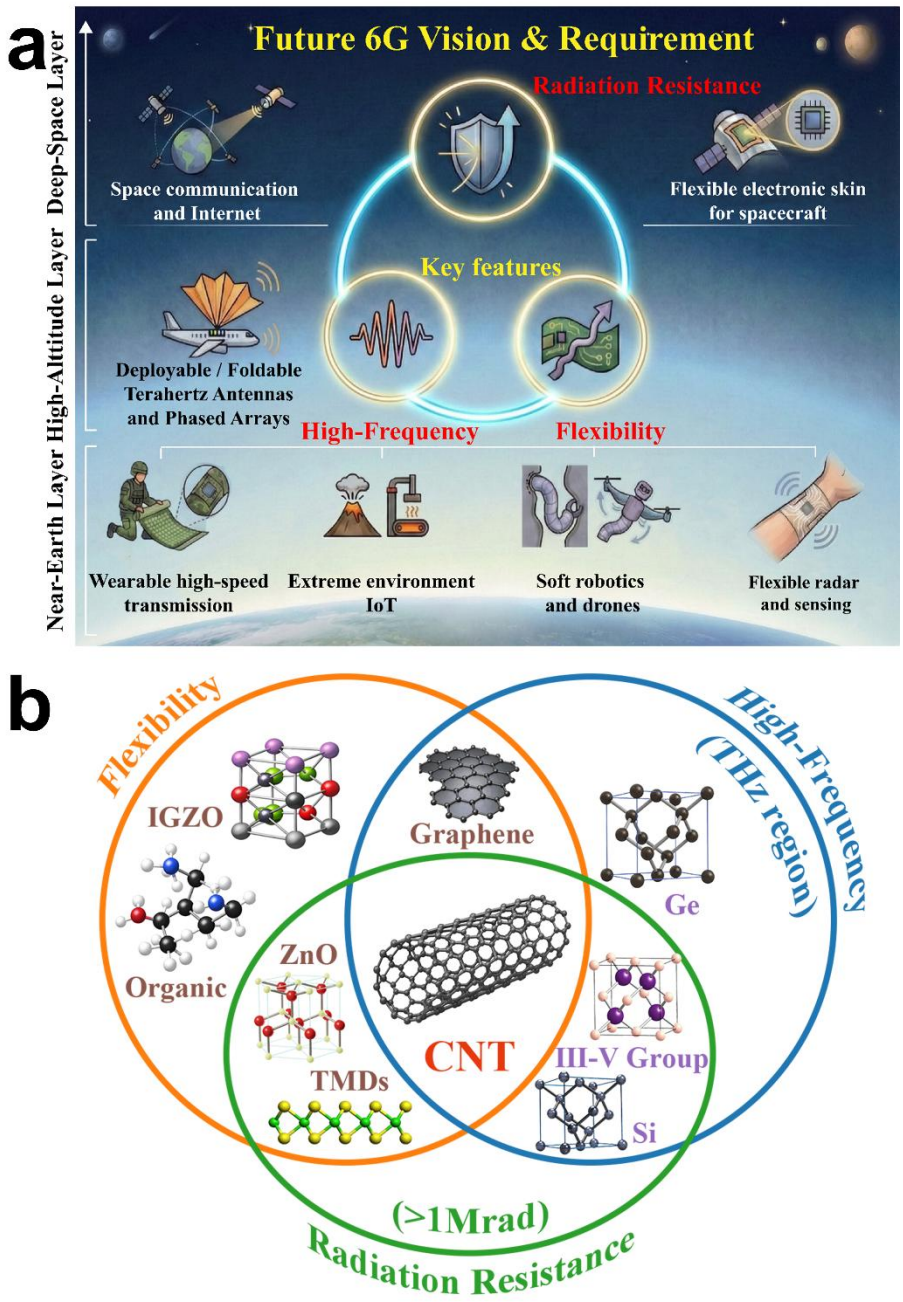


Fig. 1 | Outlook and requirements for future 6G communication. a, Representative application scenarios of future 6G technology across near-Earth, high-altitude, and deep-space environments, highlighting the demands imposed by space–air–ground integrated networks. **b,** Comparative assessment of representative semiconductor materials from 6G requirements point of view, including high-frequency, mechanical flexibility, and radiation tolerance.

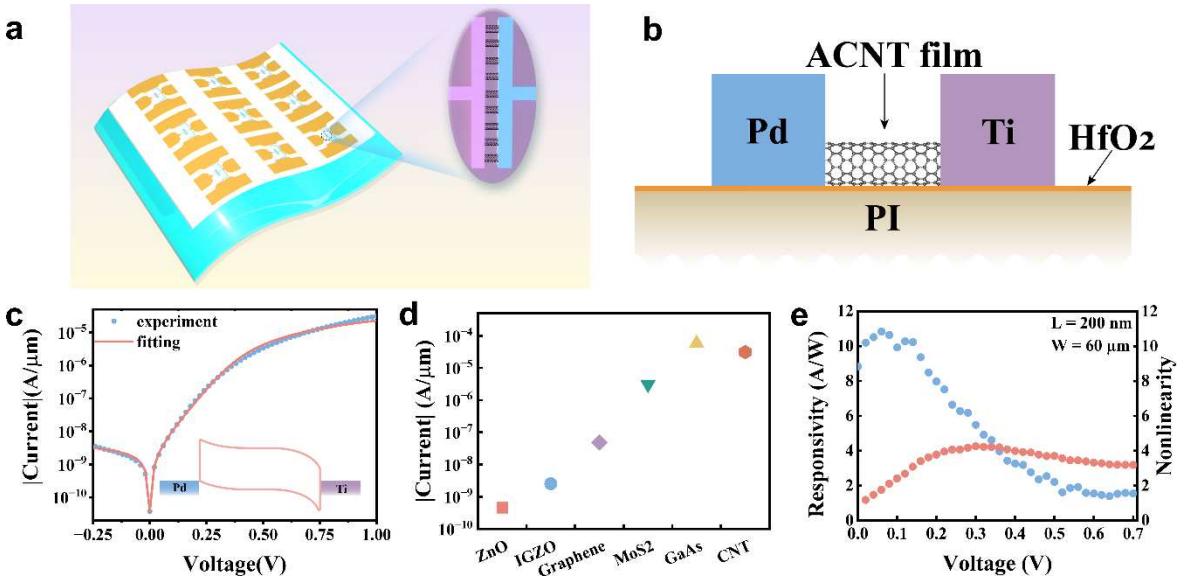


Fig. 2 | Structure and electrical characteristics of flexible Schottky diodes based on A-CNT arrays. a, A three-dimensional schematic of a flexible Schottky diode based on A-CNT arrays, featuring a ground-source-ground (G-S-G) structure. The enlarged view on the right illustrates the planar layout of the diode. **b,** A schematic of the diode on PI substrate. **c,** The direct current (d.c.) I-V characteristics of the diode, along with the fitting curve based on the Shockley diode equation. The extracted ideality factor n is 2.00, and the series resistance R_S is 11.14 Ω. The inset depicts the energy band diagram of the diode. **d,** The current responsivity of the diode at various bias voltages. The channel length and width are 200 nm and 20 μm, respectively. **e.** Benchmarking of the line current density of A-CNT array-based Schottky diodes against other flexible-material-based devices, including graphene and MoS_2, as well as hard-substrate counterparts such as ZnO and IGZO.

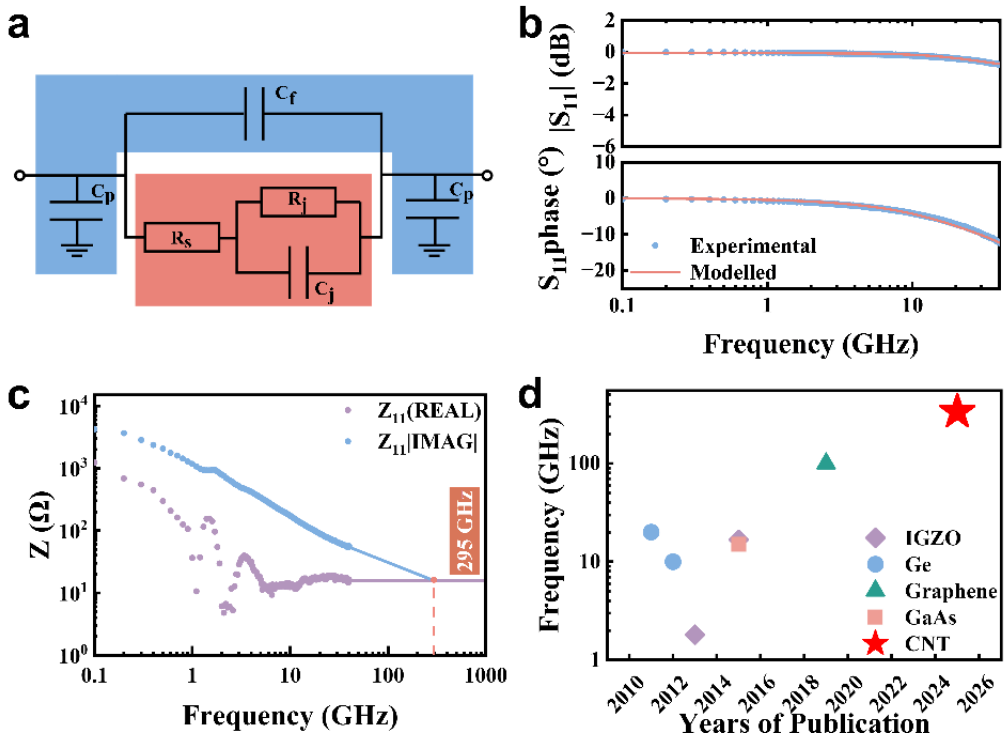


Fig. 3 | High-frequency properties of flexible Schottky diodes based on A-CNT arrays. a, Equivalent circuit of the A-CNT Schottky rectifier. **b,** Amplitude (top) and phase (bottom) of the S_{11} parameters of the flexible Schottky diode, along with the fitted results using ADS simulations. **c,** Intrinsic cutoff frequency of flexible Schottky diodes based on A-CNTs arrays with a width of 60 μm, the zero-bias $f_{c,int}$ of CNT-FSBDs is obtained by converting the measured S-parameters to Z-parameters. **d,** Benchmarking of the intrinsic cutoff frequencies of state-of-the-art Schottky diodes based on various material systems, including IGZO, Ge, Graphene and GaAs on flexible substrates.

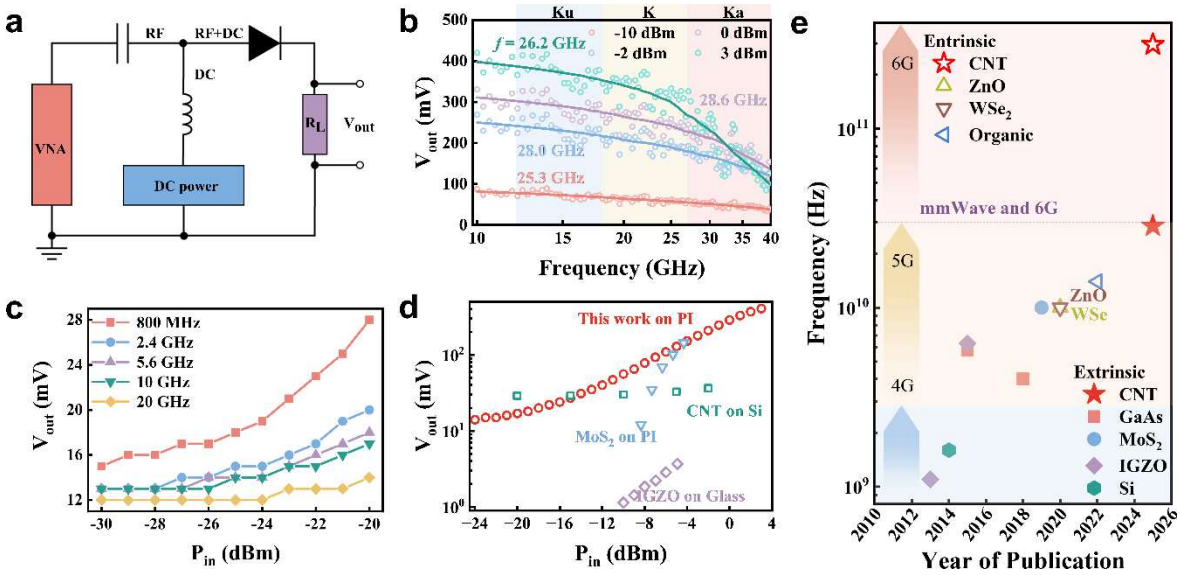


Fig. 4 | Output voltage capability of flexible Schottky diodes based on A-CNT arrays. a, Circuit diagram of the diode. The vector network analyzer (VNA) is used for measurements, and R_L denotes the load resistor. The DC power supply provides the necessary DC bias voltage. **b,** Rectified output voltage as a function of frequency for various input RF powers (−10 dBm, −2 dBm, 0 dBm, and 3 dBm). The channel width is 60 μm. At an input RF power of 3 dBm, the extrinsic cutoff frequency f_c is approximately 22.3 GHz at 0 V bias. **c,** Output voltage as a function of input RF power across five different frequencies (800 MHz, 2.4 GHz, 5.6 GHz, 10 GHz, and 20 GHz). The channel dimensions are 200 nm in length and 60 μm in width, measured at 0 V bias. **d,** Benchmarking output voltages of various materials and substrates at low RF powers ranging from −14 to −3 dBm, including CNTs on Si, MoS_2 on PI, and IGZO on glass. **e,** Benchmarking of the extrinsic cutoff frequencies (f_c) of state-of-the-art Schottky diodes based on various material systems, including GaAs, MoS_2, IGZO, and Si on flexible substrates, as well as organic semiconductors, WSe_2, and ZnO on rigid substrates. The comparison highlights the high-frequency performance advantage of A-CNT array-based diodes.

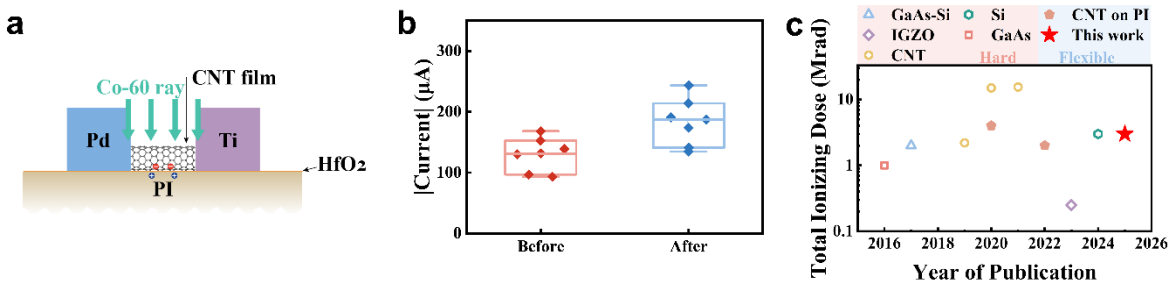


Fig. 5 | Total ionizing dose of flexible Schottky diodes based on ACNT arrays. a, Schematic diagram illustrating the irradiation mechanism for a diode. The irradiation source used is Co-60 gamma rays. **b,** Statistical analysis of the irradiation effects on seven Schottky diodes before and after exposure, highlighting the variations in key electrical parameters. The analysis includes a comparison of the diode current characteristics before and after irradiation at 1 V bias, revealing the impact of radiation-induced defects on charge transport and barrier integrity. **c,** TID tolerance comparison of electronic devices fabricated from various semiconductor materials, including GaAs-Si, Si, IGZO, GaAs, and CNT, demonstrating the superior radiation tolerance of CNT-based devices, attributed to their intrinsic defect resilience and high carrier mobility.

Supplementary Files

This is a list of supplementary files associated with this preprint. Click to download.

- YanLiSI20260403.docx